Photos: Corbis, DOI: 10.2516/ogst/2012104, IFPEN, X.

Dossier

This paper is a part of the hereunder thematic dossier published in OGST Journal, Vol. 68, No. 6, pp. 951-1113 and available online here

Cet article fait partie du dossier thématique ci-dessous publié dans la revue OGST, Vol. 68, n°6, pp. 951-1113 et téléchargeable ici

DOSSIER Edited by/Sous la direction de : **C. Barrère-Tricca**

IFP Energies nouvelles International Conference / Les Rencontres Scientifiques d'IFP Energies nouvelles

MAPI 2012: Multiscale Approaches for Process Innovation

MAPI 2012 : Approches multi-échelles pour l'innovation des procédés

Oil & Gas Science and Technology – Rev. IFP Energies nouvelles, Vol. 68 (2013), No. 6, pp. 951-1113

Oil & Gas Science and Technology – Rev. IFP Energies nouvelles, Vol. 68 (2013), No. 6, pp. 995-1005

DOI: 10.2516/ogst/2013123

IFP Energies nouvelles International Conference
Rencontres Scientifiques d'IFP Energies nouvelles

MAPI 2012: Multiscale Approaches for Process Innovation
MAPI 2012 : Approches multi-échelles pour l'innovation des procédés

Sulfur Deactivation of NO_x Storage Catalysts: A Multiscale Modeling Approach

N. Rankovic[1,2*], C. Chizallet[3], A. Nicolle[1*], D. Berthout[1] and P. Da Costa[2]

[1] *IFP Energies nouvelles, 1-4 avenue de Bois-Préau, 92852 Rueil-Malmaison - France*
[2] *Institut Jean Le Rond d'Alembert, Université Pierre et Marie Curie, UPMC Paris 6, CNRS UMR 7190, 2 place de la gare de ceinture, 78210 Saint-Cyr-l'École - France*
[3] *IFP Energies nouvelles, Rond-point de l'échangeur de Solaize, BP 3, 69360 Solaize - France*
e-mail: nikola.rankovic@aramcooverseas.com - andre.nicolle@ifpen.fr

* Corresponding authors

Résumé — Empoisonnement des matériaux de stockage des NO_x par le soufre : approche multi-échelles — Les pièges à NO_x représentent une technologie prometteuse pour la réduction des émissions d'oxydes d'azote issus des moteurs opérant en mélange pauvre. Leur utilisation est limitée par la présence de composés soufrés dans les gaz d'échappement. Le soufre contenu dans le carburant et le lubrifiant est oxydé lors de la combustion en SO_2 et SO_3. Ces oxydes de soufre présentent une forte affinité pour le matériau de stockage du piège, la formation de sulfate étant favorisée thermodynamiquement. Cette formation contribue au blocage des sites d'adsorption des NO_x et influence l'opération de l'organe de post-traitement. La modélisation moléculaire représente un outil précieux pour prédire le comportement et les performances du système catalytique. Notre étude présente une méthodologie d'exploitation des calculs *ab initio* pour la formulation de modèles cinétiques développés dans la librairie de post-traitement véhicule *IFP Exhaust*. Nous illustrons notre approche par le cas de l'adsorption de SO_3 sur un matériau modèle, BaO. Afin d'obtenir une description fidèle du matériau de stockage réel, l'adsorption de SO_3 est décrite sur plusieurs sites : terrasses, marches, crans et le site massique. Des analyses de sensibilité et de vitesses de réactions permettent d'obtenir une compréhension plus approfondie des phénomènes d'empoisonnement mis en jeu.

Abstract* — *Sulfur Deactivation of NO_x Storage Catalysts: A Multiscale Modeling Approach — *Lean NO_x Trap (LNT) catalysts, a promising solution for reducing the noxious nitrogen oxide emissions from the lean burn and Diesel engines, are technologically limited by the presence of sulfur in the exhaust gas stream. Sulfur stemming from both fuels and lubricating oils is oxidized during the combustion event and mainly exists as SO_x (SO_2 and SO_3) in the exhaust. Sulfur oxides interact strongly with the NO_x trapping material of a LNT to form thermodynamically favored sulfate species, consequently leading to the blockage of NO_x sorption sites and altering the catalyst operation. Molecular and kinetic modeling represent a valuable tool for predicting system behavior and evaluating catalytic performances. The present paper demonstrates how fundamental* ab initio *calculations can be used as a valuable source for designing kinetic models developed in the IFP Exhaust library, intended for vehicle simulations. The concrete example we chose to illustrate our*

approach was SO_3 adsorption on the model NO_x storage material, BaO. SO_3 adsorption was described for various sites (terraces, surface steps and kinks and bulk) for a closer description of a real storage material. Additional rate and sensitivity analyses provided a deeper understanding of the poisoning phenomena.

INTRODUCTION

Lean-burn engines are gaining the european market share. Their attractiveness is mainly linked to low consumption and low CO_2 emission, but also to advantageous de-tax systems existing in the EU. However, environmental concerns for pollutant emissions still remain the main drawback of lean-burning solutions. Since they operate in excess of oxygen, a removal of the unburned CO and hydrocarbons is easily achieved with a standard diesel oxidation catalyst, whereas NO_x abatement requires using advanced exhaust gas aftertreatment techniques.

One of the few technologies available on the market and capable of meeting the stringent emission legislations are the Lean NO_x Trap (LNT) catalysts [1-3]. LNT operation is based on successive rich/lean cycles. During lean phases, NO oxidation to NO_2 over precious metal sites (typically Pt, Rh, and Pd) takes place. NO_2, intrinsically more acidic than NO, then migrates toward the basic storage material where, it is converted and stored as nitrate. To regenerate the storage capacity of the trap, engine combustion is briefly switched to fuel-rich conditions, producing CO, H_2, and unburned hydrocarbons that reduce the stored nitrates to N_2. Among the storage materials proposed, barium oxide is widely accepted as the most prominent candidate for commercial vehicle de-NO_x applications. Initially intended for storage of NO_x as nitrates, its storage capacity is significantly altered in the presence of sulfur due to poisoning phenomena. SO_x (SO_2 + SO_3) are systematically generated as by-products of the combustion of organic sulfur compounds, species naturally occurring in fossil fuels. Sulfur oxides are thus inevitably present in the exhaust stream and the sulfation of BaO remains the main drawback for a large-scale implementation of LNT technologies.

Numerous experimental studies witness a greater thermodynamic stability of $BaSO_4$ in comparison to $Ba(NO_3)_2$ that leads to a preferential formation of sulfates and alters the NO_x storage capacity [4, 5]. Engine test bench essays confirm that commercial NO_x adsorbers are extremely sulfur-sensitive and that even sophisticated ultra-low-sulfur fuels containing 10 ppm S poison the NO_x storage function [6]. Exposure to SO_2 in the presence of O_2 leads to a disappearing of the carbonate IR bands on a model $Pt/Ba/Al_2O_3$ catalyst and to their progressive replacement by distinctive surface and bulk sulfate bands [7]. *In situ* infrared studies by Breen *et al.* [8] showed that barium carbonate can be replaced by barium sulfate by reaction with low concentrations of SO_2 in the presence of large quantities of CO_2 at temperatures up to 700°C. Chronologically, surface sulfates are the first to appear, followed by bulk $BaSO_4$ and bulk $Al_2(SO_4)_3$. Furthermore, the NO_x storage capacity decrease is found to be proportional to the amount of SO_2 to which the BaO-based storage material has been exposed [9]. It is commonly accepted that SO_2 undergoes oxidation to SO_3 over precious metal sites. Experiments over a $Pt/Ba/Al_2O_3$ catalyst confirm that SO_2 + O_2 exposure results in the formation of SO_3 that is being trapped as sulfate according the proposed reaction scheme [10].

$$SO_2 + 0.5\,O_2 \rightarrow SO_3$$
$$BaO + SO_3 \rightarrow BaSO_4$$

SO_3 gradually accumulated on barium sites forms $BaSO_4$, which prevents NO_x storage to take place [9, 11]. Thus, understanding the way sulfur poisoning occurs on BaO through interactions with SO_3 has aroused our interest in conducting a comprehensive multi-scale study on this matter.

Desulfation of the accumulated SO_x involves heating the catalyst to the temperature above 700°C or switching to a reducing atmosphere (CO or H_2) [12-16]. The main issue for the high-temperature desulfation is the loss of the catalytic activity caused by thermal aging (precious metal sintering and formation of $BaAl_2O_4$ [17]). Exposure to H_2 on the other hand deteriorates the storage material through formation of crystalline BaS [18].

In contrast to abundant experimental data focused on sulfur poisoning, no theoretical work fully assessing chemisorption of SO_2 or SO_3 has been conducted up to date. Most of the existing studies targeted SO_x adsorption on alkaline-earth oxides at low surface coverage [19-22]. All of them unanimously agree that both SO_2 and SO_3 readily adsorb as Lewis acids by anchoring the sulfur atom to a basic oxygen site on BaO surface to form sulfite- (SO_2 adsorption) and sulfate-like (SO_3 adsorption) surface species. Our previous studies were focused on acquiring fundamental insight into the nature of SO_3 interactions with various types of BaO surfaces

(ideal surfaces and surface defects) at high surface coverages, providing a broader picture of SO_x chemistry on BaO [23].

When it comes to kinetic models, there is a great need for developing reaction schemes based on quantified data for sulfur poisoning. Very few kinetic models for sulfur deactivation have been proposed in the literature. The most elaborated one, conceived by Dawody *et al*. [24] describes a multi-site competitive SO_x adsorption on the NO_x storage sites. According to their model, SO_2 is oxidized on Pt sites to SO_3 during the storage phase and reduced to H_2S during the regeneration in the presence of H_2. In a more recent modeling study by Olsson *et al*. [25] sulfur poisoning is described *via* SO_2 adsorption on BaO and Al_2O_3 and the subsequent oxidation to sulfate species.

Multiscale modeling of heterogeneous chemical reactions implies transposing fundamental mechanistic insights that are available from molecular modeling (DFT, force-field) onto larger scales (kinetic Monte-Carlo, mean-field approximation) intended for catalyst design. Coupled to computational fluid dynamics models they provide powerful tools for reactor conception and design. A comprehensive review on multiscale modeling approaches in heterogenous catalysis is available elsewhere [26].

The present study aims at bridging the gap between different modeling scales. The choice of the system to model in the present work is based on the reaction sequence for sulfate formation. We consider BaO to be the active storage site after surface $BaCO_3$ decomposition on which pre-oxidized SO_3 is adsorbed. Although substantial amounts of $BaCO_3$ and hydroxycarbonate coexist in equilibrium with BaO when storage material is exposed to engine exhaust, $BaCO_3$ does not act as the active storage phase on its own. Instead, detailed storage mechanisms involve CO_2 desorption prior to reaction with NO_x or SO_x. This is the motivation to consider BaO surface sites as chemically active ones in the present study.

We employed state-of-the-art Density Functional Theory (DFT) computations to obtain quantum insights on BaO–SO_3 interactions together with thermodynamic data that are not available in the literature. This information was used for conceiving kinetic model for SO_3 adsorption on BaO, implemented in the *IFP Exhaust* library. Our objective was testing the methodology of multiscale modeling in which DFT-based data obtained at the atomic level were used directly on a higher-level scale for conceiving kinetic models. As a final step, sensitivity analyses were performed to assess the importance of various modeling parameters to the sulfation mechanism.

1 METHODS

1.1 *Ab Initio* Computations

Periodic DFT calculations were carried out in the framework of the generalized gradient approximation exchange-correlation functional of Perdew and Wang PW91 [27], as implemented in VASP 4.6 package [28, 29]. The one-electron wave function was developed in a plane-wave basis set, and the interaction between core and valence electrons was described by the Projector Augmented Waves (PAW) approach [30]. A cutoff energy of 400 eV was used. The convergence criterion for the electronic Self-Consistent Field (SCF) loop is set to 1×10^{-6} eV per cell for simple structures (gas-phase molecules and solid bulks) or to 5×10^{-6} eV for supercell computations. Geometry optimizations were performed within a conjugate-gradient algorithm until the convergence criterion on forces (0.02 eV·Å^{-1}) was reached. A dipolar correction along the direction perpendicular to the slab (*z*-axis) was applied for neutralizing any spurious electrostatic interaction between the slab and its periodic images, due to the asymmetric nature of the slabs.

Velocity-scaled Molecular Dynamics (MD) were used for investigating species adsorption at higher fractional coverages, each time a surface reconstruction phenomenon was encountered. Velocities were scaled at each time step (5 fs) to the chosen temperature (600 K). The DFT calculation accuracy was decreased in order to limit computational cost. More precisely, a cutoff energy of 300 eV was used, with the convergence criterion for the electronic SCF loop set to 1×10^{-4} eV. The energetic minima obtained from the MD simulation were subsequently quenched by performing a geometry optimization at 0 K with usual accuracy parameters, and the most stable quenched structures are assumed to give the best estimate of the most energetically favorable configurations.

Raw *ab initio* data were used for quantifying the incremental stability of adsorbed states with the increasing SO_3 coverage (from $(n-1)$ to n adsorbed SO_3 molecules per cell) that we describe *via* differential adsorption energy, $\Delta_{ads}U$, defined as

$$\Delta_{ads}U = U_{\mathrm{BaO+nSO_3}} - U_{\mathrm{BaO+(n-1)\,SO_3}} - U_{\mathrm{SO_3}} \qquad (1)$$

where $U_{\mathrm{BaO+(n-1)\,SO_3}}$, $U_{\mathrm{BaO+nSO_3}}$ and $U_{\mathrm{SO_3}}$ are the energies of the adsorbed states and of SO_3 molecule, respectively. For the case of bulk $BaSO_4$ formation, the energy of formation is obtained by subtracting the calculated cohesive energy of $BaSO_4$ crystal from that of BaO and SO_3.

In the present study, we focalize on SO_3 adsorption onto three types of surface sites – ideal BaO terraces (T) and two surface irregularities: surface steps (S) and kinks (K). Further information and detailed modeling parameters of the surfaces studied within is available from our previous work [23]. The forth adsorption site considered is bulk BaO leading to the formation of crystalline $BaSO_4$. This four-site reaction scheme is summarized below.

$$R1\ SO_3 + BaO(T) \rightarrow SO_3 - BaO(T)$$
$$R2\ SO_3 + BaO(S) \rightarrow SO_3 - BaO(S)$$
$$R3\ SO_3 + BaO(K) \rightarrow SO_3 - BaO(K)$$
$$R4\ SO_3 + BaO(bulk) \rightarrow SO_3 - BaO(bulk)$$

1.2 Kinetic Model

The proposed 4-site model supposes that the adsorbate is randomly distributed on each type of surface (mean-field assumption) [26]. Coverage dynamics of the adsorbed sulfur species on the surface site i is described *via* [31, 32]

$$\frac{d\theta_{SO_3,i}}{dt} = \frac{r_i}{\Psi_i} \tag{2}$$

in which r_i (mol·m^{-3}·s^{-1}) is the rate of consumption of generation of SO_3 due to adsorption or desorption onto/from ith site. Every site has its own density, Ψ_i (mol·m^{-3}). Equation (3) describes the gaseous SO_3 source term, ω_{SO_3}

$$\omega_{SO_3} = M_{SO_3} V_\Sigma \sum_{i=1}^{N} r_i \tag{3}$$

in which N is the number of SO_3 storage site types, V_Σ is the active volume of the storage material, and M_{SO_3} is SO_3 molar weight. Reaction rates r_i are described by elementary step based reaction mechanisms. Forward reaction rate constants are described *via* the Arrhenius expression, and to assure the thermodynamic consistency of the model, the backward reactions are computed *via* the corresponding thermodynamic constants [33]

$$r_i = A_i \exp\left(-\frac{E_{a,i}}{RT}\right) \times \left(c_{SO_3}\theta_{void,i} - \frac{1}{K_{eq,i}}\left(\frac{P}{RT}\right)\theta_{SO_3,i}\right) \tag{4}$$

with A_i being the pre-exponential factor, $E_{a,i}$ the corresponding activation energy, c_{SO_3} is gas-phase SO_3 concentration, $K_{eq,i}$ the thermodynamic equilibrium constant for adsorption on ith site. Site fractions $\theta_{void,i}$ and $\theta_{SO_3,i}$ (dimensionless) describe void and SO_3 fractional coverage on ith site, respectively. The equilibrium constants are calculated from the corresponding thermodynamic data *via*

$$K_{eq,i} = \exp\left(-\frac{\Delta rH_i}{RT}\right)\exp\left(\frac{\Delta rS_i}{R}\right) \tag{5}$$

with ΔrH_i and ΔrS_i representing respectively the enthalpy and the entropy of the adsorption reaction on ith adsorption site.

1.3 Reactor Model

The kinetic scheme was implemented in a reactor model developed in the AMESim (LMS.Imagine.Lab) modeling platform, itself based on the bond-graph theory [34]. Briefly, the bond-graph approach associates capacitive elements (volume) and resistive elements (pressure drop, mass and enthalpy flow rates) for modeling multi-physical systems such as chemical reactors. Detailed architecture of the bond-graph reactor model we used is available elsewhere [35]. Its successful implementation in multi-0D kinetic modeling has been demonstrated in our previous work [36-38]. Species mass balance is computed as

$$\frac{dm_j}{dt} = \dot{m}_j^{in} - \dot{m}_j^{out} + \omega_j \tag{6}$$

in which $\dot{m}_j^{in}$ and $\dot{m}_j^{out}$ represent inlet and outlet mass flux for species j (SO_3 or the carrier gas), while ω_j stands for the chemical source term (only applicable to SO_3, Eq. 3). Note that the impact of internal transport was not taken into account in this study. In order to describe more accurately the LNT operation, the impact of internal porosity variation on the effective species diffusivity would have to be accounted for [39]. Pressure is calculated from the energy balance inside the reactor volume [35]

$$\frac{dP}{dt} = \frac{\gamma P}{m\, C_p T_g}\left(\delta\dot{Q}_{th,in} + MC_pT_g\frac{dn}{dt} + \dot{m}\delta h\right) \tag{7}$$

γ being the isentropic coefficient, T_g gas temperature, C_p gas specific heat, n is the amount of gas, M its molar mass, and $\delta\dot{Q}_{th,in}$ the internal heat transfer, calculated from the difference between gas- and solid-phase temperatures. The reactor is modeled as a fixed bed filled with BaO powder for which mass flux and superficial gas velocity v are computed from pressure drop across the bed using Darcy's law [40]

$$\frac{\Delta P}{L} = \frac{150(1-\epsilon)^2\mu}{\epsilon^3 dp^2}v \tag{8}$$

ΔP being the pressure drop, L the bed length, ϵ the bed void fraction, μ the dynamic viscosity of the fluid and dp the particle diameter.

2 RESULTS

2.1 SO_3 Adsorption on BaO: Quantum Mechanical Insights

In our previous DFT study, we thoroughly investigated SO_3 adsorption thermodynamics on several BaO surface types (terraces, steps and kink surface defects) [23]. It has been found, in line with previous theoretical studies, that SO_3 molecule adsorbs readily on basic oxygen surface sites. SO_3 acts as a multidentate ligand that tends to surround itself by a maximal number of coordination bonds with BaO. Site topology has been found to strongly influence the thermodynamics of the adsorption. When adsorbed, SO_3 molecule is strongly deformed from its original state, forming a tetrahedral environment of the S atom, characteristic of a sulfate-alike structure.

Once adsorbed on BaO surface, SO_3 molecule penetrates and restructures its environment to form bulk $BaSO_4$. With an increasing surface coverage, reconstruction phenomena are observed for the terrace adsorption. Every time a surface reconstruction was encountered during a static geometry optimization, a molecular dynamic simulation was performed to explore possibilities for a further surface reconstructions. This was the case for SO_3 adsorption on terraces at surface coverages higher than 0.5 ML (monolayer). Calculated adsorption energies are illustrated as points in Figure 1. We showed previously that steps and kinks are not strongly reconstructed upon SO_3 adsorption, contrary to terraces. However, SO_3 adsorbs strongly on these surface defects, which suggests that diffusion of sulfates only involves the terraces [23].

Further investigations of SO_3 adsorption on BaO aimed to provide an insight into adsorption kinetics. This was achieved by tracing the energetic profile of a SO_3 molecule approaching a basic O_{5C} site. For this purpose, the most stable sulfate structure obtained for the adsorption on a BaO(100) terrace was distorted by increasingly moving the molecule away from the surface along the z axis. The adsorption energy profile (*Fig. 2*) illustrates a transition from a physisorbed to a chemisorbed state. No noticeable activation barrier for a transition from the gas-phase SO_3 to a chemisorbed state was observed for this perpendicular approach. This finding is particularly interesting for the conception of the kinetic model, allowing us to postulate a non-activated surface SO_3 adsorption. Note finally that the reactivity – eventually migration – of surface oxygen atoms cannot be excluded, although it is not sufficient to explain the formation of bulk sulfate requiring S atoms. We are presently working on the interaction of O_2 and SO_2 with BaO, which should allow us to draw conclusions on the importance of the migration of peroxide at the surface.

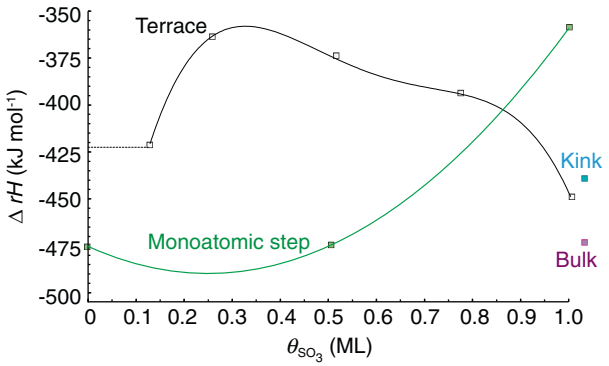

Figure 1

Standard (101.325 kPa, 298.15 K) SO_3 adsorption enthalpies (ΔrH) on various types of BaO sites (terraces, steps, kinks and bulk sites) as a function of SO_3 fractional coverage, θ_{SO_3}. Points represent the results obtained from *ab initio* calculations, lines are the interpolations to all fractional coverage values.

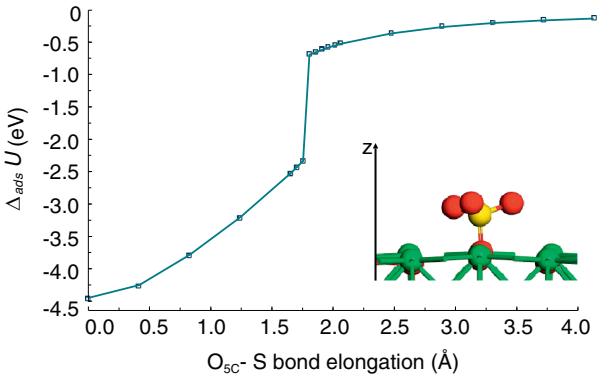

Figure 2

SO_3 molecule adsorbed onto a basic oxygen site of the BaO surface. Energetic profile for the SO_3 –BaO(100) system as the molecule approaches the basic surface site along the z axis. The bond elongation is relative to the equilibrium bond length of 1.57 Å.

2.2 Kinetic Study

Following our *ab initio* studies [23], we modeled SO_3 adsorption on three types of surface sites (terraces, steps

and kinks) and on bulk BaO site using a global modeling approach. Storage material was represented as a BaO particle with a storage capacity of 3.89×10^4 mol·m^{-3}, based on the elementary BaO cell volume of 170.67 Å^3 and four BaO formula units per cell. In line with BaO dispersions (around 33%) measured by XRD for a typical model $Pt/Ba/Al_2O_3$ formulation [41], we consider that one third of the storage sites are surface sites, and the two thirds represent bulk BaO. To obtain the speciation of various surface sites, it is helpful to look at the values of surface energies relative to every kind of surface we are interested in. These values are available from our DFT studies [23] and we postulate the abundance of each surface site inversely proportional to its surface energy value (*Fig. 3*).

We used the thermodynamic data extracted from the *ab initio* studies, to conceive a kinetic model that describes SO_3 adsorption on BaO particle. First parameters that we discuss are the pre-exponential factors used for the global simulation. Surface adsorptions are modeled with a pre-exponential factor of 1.0×10^6 s^{-1}, corresponding to a typical transition state theory-based value for an immobile precursor molecular adsorption [42]. The pre-exponential factor for adsorption on bulk BaO sites of 1.0×10^7 s^{-1} was based on a typical value for a mobile precursor mediated adsorption, knowing that the formation of bulk sulfate commences with a surface adsorption, and therefore requires the molecule to diffuse into deeper layers. The value we discuss for bulk adsorption is relatively close to the one proposed in the study of Dawody *et al.* [24] for SO_3 adsorption on bulk site. The numerical value attributed by the authors is 2.33×10^4 m^3·mol^{-1}·s^{-1} or, expressed as a turnover rate, 9.1×10^8 s^{-1}.

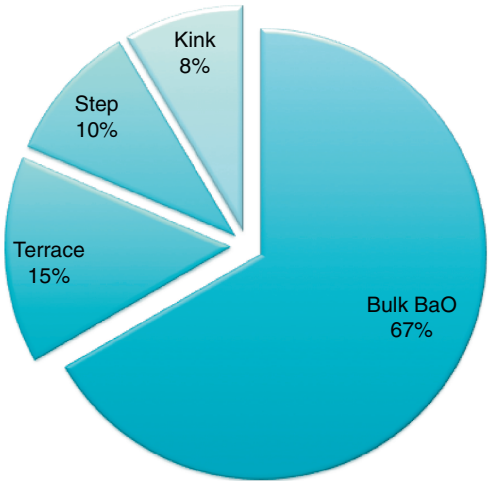

Figure 3

Speciation of BaO sites used in global simulations.

Based on the non-activated approach of a SO_3 molecule to a basic O site (*Fig. 2*), activation energies for SO_3 adsorption on surfaces are kept at zero. Formation of bulk $BaSO_4$ however requires a SO_3 molecule to penetrate into the crystal structure. The activation energy proposed by Dawody *et al.* [10] (1 kJ·mol^{-1}) seems fairly low for passing a barrier for breaking bulk Ba–O bonds inside the crystal structure. Instead, we propose a value of 80.5 kJ·mol^{-1}, that is approximately 1/6 of the atomization energy of crystal BaO [43].

With the adsorption energies for each of the four sites in hand, we based all adsorption enthalpies solely on our previous DFT data [23]. Adsorption enthalpy ΔrH is deduced directly from the corresponding adsorption energy, $\Delta_{ads}U$ (Eq. 1) using the fundamental thermodynamic relation:

$$\Delta rH = \Delta_{ads}U + PV \tag{9}$$

where the term PV is substituted with RT, attributing all volume change due to the adsorption event to the volume of the adsorbed gas molecules. In other terms, the condensed phase volume variations are considered neglectable in front of the gas volume change.

For the case of SO_3 adsorption on terraces and steps, we worked out an entire range of adsorption energies as a function of SO_3 fractional coverage, θ_{SO_3}. The values are extrapolated over the 0-1 ML fractional coverage range using an appropriate polynomial fit (*Fig. 1*, *Tab. 1*). Since the supercell model used in the periodic DFT approach contains eight surface Ba atoms, the lowest fractional coverage value we model is 1/8, or 0.125 ML. For the values below 0.125 ML, we confidently postulate no or very little lateral interactions between adsorbed molecules, and use the same adsorption enthalpy value from 0.125 ML to all lower coverages (*Fig. 1*, dashed line).

Adsorption entropies used in the global model are based on the estimation of the changes in the molecule's degrees of freedom during the adsorption event. Given the nature of SO_3 adsorption (non-activated and highly thermodynamically favorable), the adsorbed species may be described as a completely localized species. The entropy change between the gas phase and a localized species can be described by the following equation:

$$\Delta rS = -S_{tr,3D} - S_{rot,3D} \tag{10}$$

where $S_{tr,3D}$ and $S_{rot,3D}$ represent the translational and the rotational contribution to the entropy of SO_3 molecule in the gas phase, respectively. The thermochemistry

TABLE 1
Kinetic and thermodynamic parameters for SO_3 adsorption on different BaO sites

Site	Terrace	Step (S)	Kink (K)	Bulk
A (s^{-1})	1.0×10^6	1.0×10^6	1.0×10^6	1×10^7
E_a ($kJ \cdot mol^{-1}$)	0	0	0	80.5
ΔrH ($kJ \cdot mol^{-1}$)	-420 for $\theta_{SO_3} \leq 0.125$ ML and $-2\,587 \times \theta^4_{SO_3} + 6\,175 \times \theta^3_{SO_3} - 5\,294 \times \theta^2_{SO_3} + 1\,836 \times \theta_{SO_3} - 579$ for 0.125 ML $< \theta_{SO_3} \leq 1$ ML	$232 \times \theta^2_{SO_3} - 116 \times \theta_{SO_3} - 475$	–469	–437
ΔrS ($J \cdot mol^{-1} \cdot K^{-1}$)	–246	–246	–246	–314

of the SO_3 molecule in gas phase was determined thanks to the integration of partition functions, according to the ideal gas model, after a frequency mode determination performed with Dmol program (distributed by *Accelrys*). To the adsorption on a bulk site is attributed an entropy change based on the data extracted from *Outokumpu HSC Chemistry* (distributed by *Outokumpu Research Oy*). All ΔrS values are postulated to be temperature-independent.

The kinetic model was tested in the experimental conditions summarized in Table 2. The storage material (BaO) is packed within a cylinder tube and exposed to a 200 ppm SO_3 inlet in He carrier gas at 25°C during 2 500 s. The storage phase is followed by a temperature ramp of 5°C min^{-1} allowing stored SO_3 to desorb. Obtained SO_3 profile is given in Figure 4.

As seen from Figure 5, SO_3 desorption starts from 800°C, a temperature slightly higher than typical desulfation temperatures for $Pt/Rh/BaO/CeO_2/Al_2O_3$ catalysts [15]. A higher desulfation temperature can be expected given the fact that synergic effects between noble metal and storage material may facilitate thermal decomposition of $BaSO_4$ [16]. To get a better insight into the desulfation kinetics, we followed reaction rates and surface coverages during the temperature ramp. Results given in Figure 6 reveal that, at room temperature, all surface sites are subject to poisoning, whereas bulk websites do not react yet. During the temperature increase and after having reached 620°C, SO_3 migrates from terrace sites toward void step and divacancy sites, resulting in an increase of their coverage values (*Fig. 7*). Migration from terrace sites continues at higher temperatures, conveying SO_3 to bulk sites. Simultaneously, but to a lesser extent, step sites also contribute to bulk $BaSO_4$ formation. The balance SO_3 desorbed from terraces is seen as a small, sharp peak at 780°C. According to our rate analysis, the peak in SO_3 signal at 985°C is a result of bulk desorption, superposed with minor contributions of terrace and step desorptions. The final two SO_3 signals arise from kink and step desorptions, respectively.

The evolution of surface and bulk saturation during the temperature ramp is consistent with the reaction rate

TABLE 2
Modeled conditions and setup for SO_3 storage and TPD on BaO

Parameter	Value
Gas composition	Storage phase: 200 ppm SO_3 in He during 2 500 s TPD phase: He
Volumetric flow rate (SCCM)	6.0×10^3
Reactor length (mm)	14.0
Reactor diameter (mm)	7.0
BaO volume (mm^3)	216
BaO storage capacity ($mol\ m^{-3}$)	3.89×10^4
T profile	Storage: 25°C TPD: 25-1 000°C ramp, 5°C·min^{-1}

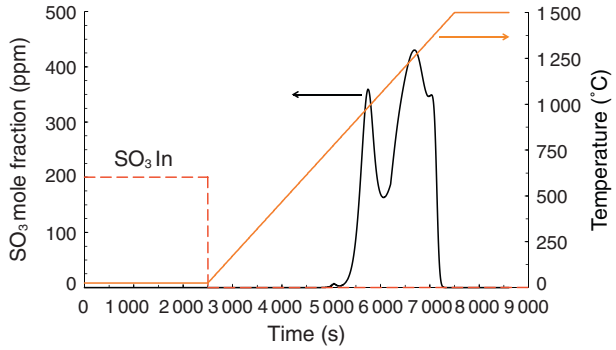

Figure 4

SO_3 inlet (red) and outlet (black) concentration profiles during the storage and temperature ramp experiment, in the conditions presented in Table 2. For illustration purposes, temperature profile is also given (orange).

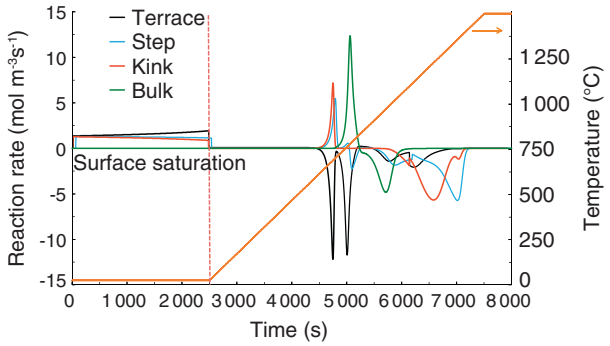

Figure 6

Reaction rates *versus* time during the storage–TPD experiment. The end of the SO_3 storage phase is delimited with a dashed line. Temperature profile is given in orange.

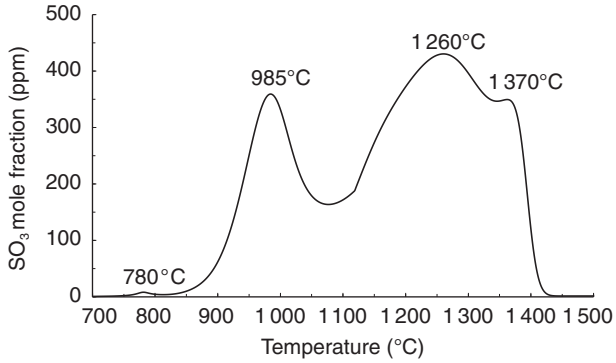

Figure 5

A closer look to the SO_3 outlet concentration profile *versus* temperature during the temperature ramp experiment.

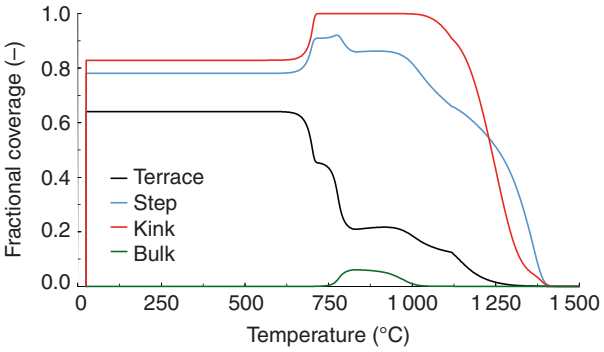

Figure 7

SO_3 fractional coverages as a function of temperature during the storage–TPD experiment.

analysis (*Fig. 7*). It can be seen that during the exposure to SO_3 at room temperature, three surface sites interact readily with SO_3, and thus their fractional coverages reach values different from zero. The initial transfer of SO_3 from terrace to step and kink sites is observed above 620°C as the terrace coverage decreases with a simultaneous increase in the step and kink coverages. A subsequent transfer from terraces to bulk is marked as a sharp decrease in terrace coverage above 710°C leading to a formation of bulk $BaSO_4$. As a final step of the desorption mechanism, on line with rate analyses, surface step and kink desulfation take place after bulk and terrace depopulation, liberating the last traces of SO_3.

Further assessment of the storage-desorption mechanism was made available through sensitivity analyses performed on the parameters with the highest degree of uncertainty. The sensitivity analysis was done in the storage conditions similar to those in Table 2, but with 400 ppm SO_3 inlet during 2 500 s. The increase in SO_3 concentration from original 200 to 400 ppm was necessary to operate in excess of SO_3 so to saturate the storage material. This way, the total quantity of stored SO_3 obtained in different scenarios by increasing independently the original value of each parameter for 10% can be compared directly to the original storage scenario. The results are depicted in Figure 8. We were mainly interested in the parameters that we adopted from the literature

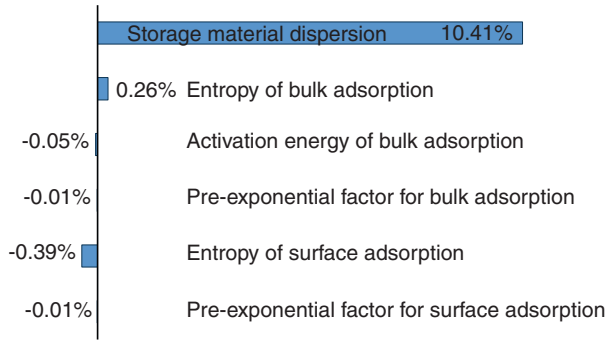

Figure 8

Results of the sensitivity studies for the storage of 400 ppm SO_3 over BaO during which various model parameters were successively increased for 10% and the quantity of stored SO_3 compared to that obtained in the original scenario.

(pre-exponential factors, A_i) and in those that were estimated in Dmol (adsorption entropies, ΔrS_i). We also examined the impact of the storage material dispersion (*i.e.*, quantity of exposed surface sites as opposed to the total number of sites). Interestingly, the sensitivity analysis shows that in our conditions the dispersion has the greatest impact on the storage properties. The amount to stored SO_3 increases linearly with a dispersion increase. This leads to a conclusion that among all simulation parameters with a high degree of uncertainty, dispersion plays the most relevant role. Consequently, controlling BaO dispersion during catalyst preparation is of primary interest for sulfur storage properties.

CONCLUSIONS

In summary, the multiscale modeling study presented in this paper was based on our previous work on SO_3 adsorption on BaO. Transposing the kinetic model proposed within as a part of the global picture into real engine exhaust operating conditions would require taking into account $BaCO_3$ formation and decomposition prior to sulfate formation to predict effectively the actual LNT operation. *Ab initio* quantum mechanical calculations were performed to elucidate the thermodynamics for SO_3 adsorption on BaO surfaces and bulk. We then focused on transposing the results of the *ab initio* calculations to a mean-field kinetic model implemented in *IFP Exhaust* library. The paper shows the main assumptions that have been made for overcoming the gap between the two scales. Further *ab initio* calculations could provide valuable kinetic data such as pre-exponential factors that were taken from the literature for the present study. This approach allows us to simulate SO_3 concentration profile obtained in a TPD experiment subsequent to SO_3 storage. The analysis of the adsorption/desorption scenarios was made through comparing reaction rates and species fractional coverages. BaO(100) terraces were found to be at the crossroads of bulk sulfate formation and a SO_3 provider for surface defects.

Sensitivity analysis performed on the original storage scenario provided us a deeper insight into the most relevant kinetic factors. The dispersion of the BaO storage material turns out to be the most important parameter for SO_3 adsorption prediction. A comparison with experimental data would prove useful to better judge the validity of the kinetic model we proposed. Moreover, the thermokinetics of the reaction of O_2 and SO_2 (present in the exhaust stream) with BaO will be compared in the future to that of SO_3 adsorption in order to assess the actual contribution of these steps to sulfate formation. Kinetic modeling stands for an appropriate tool to identify the preferential pathway.

ACKNOWLEDGMENTS

HPC resources from IFPEN and GENCI–CINES (Grant 2011-ifp6134) used for the present study are gratefully acknowledged.

REFERENCES

1 Epling W.S., Campbell L.E., Yezerets A., Currier N.W., Parks J.E. (2004) Overview of the Fundamental Reactions and Degradation Mechanisms of NO_x Storage/Reduction Catalysts, *Catal. Rev. Sci. Eng.* **46**, 163-245.

2 Roy S., Baiker A. (2009) NO_x Storage-Reduction Catalysis: From Mechanism and Materials Properties to Storage-Reduction Performance, *Chem. Rev.* **109**, 4054-4091.

3 Granger P., Parvulescu V.I. (2011) Catalytic NO_x Abatement Systems for Mobile Sources: From Three-Way to Lean Burn after-Treatment Technologies, *Chem. Rev.* **111**, 3155-3207.

4 Poulston S., Rajaram R.R. (2003) Regeneration of NO_x trap catalysts, *Catal. Today* **81**, 4, 603-610.

5 Sedlmair C., Seshan K., Jentys A., Lercher J.A. (2002) Studies on the deactivation of NO_x storage-reduction catalysts by sulfur dioxide, *Catal. Today* **75**, 1-4, 413-419.

6 Dementhon J.B., Colliou T., Martin B., Bouchez M., Guyon M., Messaoudi I., Noirot R., Michon S., Gérenet C., Pierron L. (2003) Application of NO_x Adsorber to Diesel Depollution: Performances and Durability, *Oil & Gas Sciemce and Technology – Rev. IFP* **58**, 129-149.

7 Malpartida I., Larrubia-Vargas M.A., Alemany L.J., Finocchio E., Busca G. (2008) Pt–Ba–Al_2O_3 for NO_x storage and reduction: Characterization of the dispersed species, *Appl. Catal. B: Env.* **80**, 3-4, 214-225.

8 Breen J.P., Marella M., Pistarino C., Ross J.R.H. (2002) Sulfur-tolerant NO_x storage traps: an infrared and thermodynamic study of the reactions of alkali and alkaline-earth metal sulfates, *Catal. Lett.* **80**, 123-128.

9 Engström P., Amberntsson A., Skoglundh M., Fridell E., Smedler G. (1999) Sulphur dioxide interaction with NO_x storage catalysts, *Appl. Catal. B: Env.* **22**, 4, L241-L248.

10 Dawody J., Skoglundh M., Olsson L., Fridell E. (2005) Sulfur deactivation of Pt/SiO_2, $Pt/BaO/Al_2O_3$, and BaO/Al_2O_3 NO_x storage catalysts: Influence of SO_2 exposure conditions, *J. Catal.* **234**, 1, 206-218.

11 Mahzoul H., Limousy L., Brilhac J.F., Gilot P. (2000) Experimental study of SO_2 adsorption on barium-based NO_x adsorbers, *J. Anal. Appl. Pyrolysis* **56**, 2, 179-193.

12 Kim D.H., Szanyi J., Kwak J.H., Szailer T., Hanson J., Wang C.M., Peden C.H.F. (2006) Effect of Barium Loading on the Desulfation of $Pt\text{-}BaO/Al_2O_3$ Studied by H_2 TPRX, TEM, Sulfur K-edge XANES, and *in Situ* TR-XRD, *J. Phys. Chem. B* **110**, 21, 10441-10448.

13 Luo J.-Y., Kisinger D., Abedi A., Epling W.S. (2010) Sulfur release from a model $Pt/Ba/Al_2O_3$ Diesel oxidation catalyst: Temperature-programmed and step-reponse techniques characterization, *Appl. Catal. A: Gen.* **383**, 182-191.

14 Parks J., Huff S., Pihl J., Choi J.-S., West B. (2005) *Nitrogen Selectivity in Lean NO_x Trap Catalysis with Diesel Engine In-Cylinder Regeneration*, *SAE Technical Paper* 2005-01-3876.

15 Rohr F., Göbel U., Kattwinkel P., Kreuzer T., Müller W., Philipp S., Gélin P. (2007) New insight into the interaction of sulfur with Diesel NO_x storage catalysts, *Appl. Catal. B: Env.* **70**, 1-4, 189-197.

16 Ji Y., Easterling V., Graham U., Fisk C., Crocker M., Choi J.-S. (2011) Effect of aging on the NO_x storage and regeneration characteristics of fully formulated lean NO_x trap catalysts, *Appl. Catal. B: Env.* **103**, 3-4, 413-427.

17 Szailer T., Kwak J.H., Kim D.H., Szanyi J., Wang C., Peden C.H.F. (2006) Effecs of Ba loading and calcination temperature on $BaAl_2O_4$ formation for BaO/Al_2O_3 NO_x storage and reduction catalysts, *Catal. Today* **114**, 86-93.

18 Elbouazzaoui S., Corbos E.C., Courtois X., Marecot P., Duprez D. (2005) A study of the deactivation by sulfur and regeneration of a model NSR $Pt/Ba/Al_2O_3$ catalyst, *Appl. Catal. B: Env.* **61**, 3-4, 236-243.

19 Pacchioni G., Ricart J.M., Illas F. (1994) *Ab Initio* Cluster Model Calculations on the Chemisorption of CO_2 and SO_2 Probe Molecules on MgO and CaO (100) Surfaces. A Theoretical Measure of Oxide Basicity, *J. Am. Chem. Soc.* **116**, 22, 10152-10158.

20 Schneider W.F. (2004) Qualitative Differences in the Adsorption Chemistry of Acidic (CO_2, SO_x) and Amphiphilic (NO_x) Species on the Alkaline Earth Oxides, *J. Phys. Chem. B* **108**, 1, 273-282.

21 Schneider W.F., Li J., Hass K.C. (2001) Combined Computational and Experimental Investigation of SO_x Adsorption on MgO, *J. Phys. Chem. B* **105**, 29, 6972-6979.

22 Karlsen E.J., Nygren M.A., Pettersson L.G.M. (2003) Comparative Study on Structures and Energetics of NO_x, SO_x, and CO_x Adsorption on Alkaline-Earth Metal Oxides, *J. Phys. Chem. B* **107**, 31, 7795-7802.

23 Rankovic N., Chizallet C., Nicolle A., Da Costa P. (2012) A molecular approach for unraveling surface phase transition: sulfation of BaO as a model NO_x trap, *Chem. Eur. J.* **18**, 10511-10514.

24 Dawody J., Skoglundh M., Olsson L., Fridell E. (2007) Kinetic modelling of sulfur deactivation of $Pt/BaO/Al_2O_3$ and BaO/Al_2O_3 NO_x storage catalysts, *Appl. Catal. B: Env.* **70**, 1-4, 179-188.

25 Olsson L., Fredriksson M., Blint R.J. (2010) Kinetic modeling of sulfur poisoning and regeneration of lean NO_x traps, *Appl. Catal. B: Env.* **100**, 1-2, 31-41.

26 Salciccioli M., Stamatakis M., Caratzoulas S., Vlachos D. G. (2011) A review of multiscale modeling of metal-catalyzed reactions: Mechanism development for complexity and emergent behavior, *Chem. Eng. Sci.* **66**, 4319-4355.

27 Perdew J.P., Wang Y. (1992) Accurate and simple analytic representation of the electron-gas correlation energy, *Phys. Rev. B* **45**, 23, 13244-13249.

28 Kresse G., Hafner J. (1994) *Ab initio* molecular-dynamics simulation of the liquid-metal-amorphous-semiconductor transition in germanium, *Phys. Rev. B* **49**, 20, 14251-14269.

29 Kresse G., Furthmüller J. (1996) Efficiency of *ab-initio* total energy calculations for metals and semiconductors using a plane-wave basis set, *Comput. Mater. Sci.* **6**, 1, 15-50.

30 Kresse G., Joubert D. (1999) From ultrasoft pseudopotentials to the projector augmented-wave method. *Phys. Rev. B* **59**, 3, 1758-1775.

31 Koop J., Deutschmann O. (2009) Detailed surface reaction mechanism for Pt-catalyzed abatement of automotive exhaust gases, *Appl. Catal. B: Env.* **91**, 1-2, 47-58.

32 Thormann J., Maier L., Pfeifer P., Kunz U., Deutschmann O., Schubert K. (2009) Steam reforming of hexadecane over a Rh/CeO2 catalyst in microchannels: Experimental and numerical investigation, *Int. J. Hydrogen Energy* **34**, 12, 5108-5120.

33 Mhadeshwar A.B., Wang H., Vlachos D.G. (2003) Thermodynamic Consistency in Microkinetic Development of Surface Reaction Mechanisms, *J. Phys. Chem. B* **107**, 12721-12733.

34 Paynter H.M. (1961) *Analysis and Design of Engineering Systems*, MIT Press.

35 Mauviot G., Le Berr F., Raux S., Perretti F., Malbec L.M., Millet C.N. (2009) 0D Modelling: a Promising Means for Aftertreatment Issues in Modern Automotive Applications, *Oil & Gas Sciemce and Technology – Rev. IFP* **64**, 285-307.

36 Rankovic N., Nicolle A., Da Costa P. (2010) Detailed Kinetic Modeling Study of NO_x Oxidation and Storage and their Interactions over $Pt/Ba/Al_2O_3$ Monolith Catalysts, *J. Phys. Chem. C* **114**, 7102-7111.

37 Rankovic N., Nicolle A., Berthout D., Da Costa P. (2010) Extension of a kinetic model for NO oxidation and NO_x storage to fixed-bed $Pt/Ba/Al_2O_3$ catalysts, *Catal. Commun.* **12**, 1, 54-57.

38 Rankovic N., Nicolle A., Berthout D., Da Costa P. (2011) Kinetic modeling study of the oxidation of carbon monoxide – hydrogen mixtures over Pt/Al_2O_3 and Rh/Al_2O_3 catalysts, *J. Phys. Chem. C* **115**, 20225-20236.

39 Tuttlies U., Schmeisser V., Eigenberger G. (2004) A mechanistic simulation model for NO_x storage catalyst dynamics, *Chem. Eng. Sci.* **59**, 4731-4738.

40 Stephen Whitaker (1986) Flow in Porous Media I: A theoretical derivation of Darcy's law, *Transport Porous Med.* **1**, 3-25.

41 Scotti A., Nova I., Tronconi E., Castoldi L., Lietti L., Forzatti P. (2004) Kinetic Study of Lean NO_x Storage over the Pt-Ba/Al_2O_3 System, *Ind. Eng. Chem. Res.* **43**, 4522-4534.

42 Dumesic J.A., Rudd D.F., Aparicio L.M., Rekoske J.E., Trevino A.A. (1993) *The Micokinetics of Heterogeneous Catalysis*, American Chemical Society, Washington, DC.

43 Fuentealba P., Savin A. (2000) Electronic Structure and Bonding in the Ground State of Alkaline-Earth-Metal Monoxides and Carbides, *J. Phys. Chem. A* **104**, 10882-10886.

Manuscript accepted in February 2013
Published online in September 2013